VYSOKÉ UČENÍ TECHNICKÉ V BRNĚ
FAKULTA ELEKTROTECHNIKY A KOMUNIKAČNÍCH TECHNOLOGIÍ ÚSTAV TEORETICKÉ A EXPERIMENTÁLNÍ ELEKTROTECHNIKY

Ing. Radim Kořínek

IMPLEMENTATION OF DIXON METHODS FOR PRECLINICAL MR IMAGING AT HIGH FIELDS

IMPLEMENTACE DIXONOVÝCH TECHNIK PRO PREKLINICKÉ MR ZOBRAZOVÁNÍ NA VYSOKÝCH POLÍCH

ZKRÁCENÁ VERZE DISERTAČNÍ PRÁCE

ABRIDGED DOCTORAL THESIS

Obor: Teoretická elektrotechnika

Školitel: prof. Ing. KAREL BARTUŠEK, DrSc.

Rok obhajoby: 2015

ABSTRACT

Preclinical magnetic resonance (MR) imaging in small animals is a very popular procedure that requires a higher sensitivity, given the small size of the subjects. A higher sensitivity can be reached when an MR imaging system with a high magnetic field is used (e.g., 4.7 T or higher). The benefits of such sensitivity include, for example, a higher resolution, an improved signal-to-noise ratio (SNR), an increased chemical shift, and a longer T_1 longitudinal relaxation time. On the other hand, a high field causes stronger static magnetic field deformation along the borders between tissues with different susceptibilities, and it also results in the shortening of the T_2 transversal relaxation.

Adipose tissue is significantly contained in the human (or mammal) body and is primarily used to store energy in the form of fat. This tissue can be classified into white and brown subsets. Brown adipose tissue is found mainly in new-born children, and a certain (yet very small) amount of such tissue can be traced also in adults. White adipose tissue then ensures the storage of fat as a source of energy. Furthermore, white adipose tissue produces adipokines, hormones, and many other substances important for metabolism. Generally, fat can be regarded as a biomarker in the case of specific diseases (obesity, steatosis – fatty liver disease, and others). Thus, the quantification of fat is a precondition for correct diagnosis. MR imaging comprises a special group of methods for water-fat separation; these methods are referred to as Dixon methods and utilize the principle of chemical shift.

In this thesis, a new T_2 – weighted sequence for Dixon acquisition is introduced (Chapter 4). The proposed sequence is a very time-effective three-point (3PD) method. The newly proposed sequence of fast triple spin echo Dixon (FTSED) is derived from the original fast spin echo sequence (FSE). Such modification of the original FSE sequence leads to a novel FTSED sequence, where three images are acquired simultaneously without any increase of the total acquisition time. The discussed sequence was successfully implemented on a 9.4 T MR imaging system at the Institute of Scientific Instruments, ASCR Brno. The acquired data were calculated through the use of the IDEAL (iterative decomposition of water and fat with echo asymmetry and least-squares estimation) algorithm. The results of the computation are water and fat images, and the fat fraction (FF) can be calculated from these. The sequence was successfully tested in a rat. The successful FTSED implementation on a 9.4 T MR imaging system enables this method to be used in low-field MR imaging systems.

KEYWORDS

Magnetic resonance imaging; the Dixon method; fast triple spin echo Dixon; FTSED; high field; preclinical research; iterative decomposition.

ABSTRAKT

Preklinické magneticko-rezonanční (MR) zobrazování na malých zvířatech je velmi aktuální a vyžaduje, vzhledem k rozměrům těchto zvířat, vyšší citlivost. Vyšší citlivosti lze dosáhnout použitím MR systému s vysokým základním magnetickým polem (např. 4,7 T a výše). Vyšší citlivost přináší výhody v podobě možnosti vyššího rozlišení, lepší poměr signál-šum, větší chemický posuv, prodloužení longitudinální relaxace (T_1), atd. Na druhou stranu vyšší magnetické pole znamená větší deformace základního magnetického pole na rozhraních tkání s rozdílnou susceptibilitou a zkrácení transverzální relaxace (T_2).

Tuková tkáň je významně zastoupena v lidském těle a primárně sloužící pro uchovávání energie ve formě tuků. Tukovou tkáň lze rozdělit na hnědou a bílou tukovou tkáň. Hnědá tuková tkáň se vyskytuje hlavně u novorozenců, ale může být ve velmi malém množství také u dospělých jedinců. Bílá tuková tkáň je určena pro ukládání tuků, které slouží jako zdroj energie. Kromě toho bílá tuková tkáň produkuje adipokiny, hormony a mnoho dalších látek důležitých pro náš metabolizmus. Tuk lze obecně považovat jako biomarker při určitých nemocech (obezita, steatóza jater, a další). Z tohoto důvodu je kvantifikace tuku velmi důležitá pro správnou diagnózu. V MR zobrazování je speciální skupina metod pro separaci vody a tuku. Tyto metody se nazývají Dixonovy metody a jejich princip je založen na chemickém posuvu.

V této práci je popsána nová T_2-váhovaná sekvence pro Dixonovu akvizici (Kapitola 4). Navržená sekvence je z hlediska akviziční doby velmi efektivní a řadí se mezi tříbodové Dixonovy (3PD) techniky. Nově navržená sekvence fast triple spin echo Dixon (FTSED) vychází z původní sekvence rychlého spinového echa (FSE). Modifikací původní sekvence FSE vedla ke vzniku nové sekvence FTSED, která umožňuje získat tři obrazy během jediné akvizice, bez toho aniž bychom prodloužili celkovou dobu měření. Sekvence byla úspěšně implementována na 9,4 T MRI systém na Ústavu přístrojové techniky v Brně. Získaná data byla pak zpracována iterativně pomocí algoritmu IDEAL (iterative decomposition of water and fat with echo asymmetry and least-squares estimation). Výsledkem jsou separátní obrazy vody a tuků, z kterých lze vypočítat mapy frakce tuku (FF-mapy). Sekvence byla ověřena na fantomech a poté byla odzkoušena potkanovi. Úspěšná implementace této metody na 9,4 T MRI systému znamená, že může být použita také na MR zobrazovacích systémech s nižšími magnetickými poli.

KLÍČOVÁ SLOVA

Zobrazování magnetickou rezonancí; Dixonova metoda; fast triple spin echo Dixon; FTSED; vysoké pole; preklinický výzkum; iterativní dekompozice.

PODĚKOVÁNÍ

Tato práce vznikla za finanční podpory Národního programu udržitelnosti I (NPU-I), projekt LOL1212.

Děkuji vedoucímu diplomové práce prof. ing. Karlu Bartuškovi, DrSc. za účinnou metodickou, pedagogickou a odbornou pomoc a další cenné rady při zpracování mé dizertační práce. Dále bych chtěl poděkovat Ústavu přístrojové techniky AV ČR, v. v. i. v Brně a vedoucímu NMR oddělení Ing. Zenonovi Starčukovi (jr), CSc. za možnost přístupu na 9,4 T MRI systém, na který byla implementována a odzkoušena navržená metoda.

V Brně dne ....

(podpis autora)

Table of content

1. Introduction

MRI is a significant diagnostic method for clinical medicine, and it chiefly provides excellent contrast between soft tissues in dependence on the molecular bonding between water/fat and the examined tissue. Fat often forms a substantial part of the human body and can be a significant biomarker [1] of the patient's health. Hence, fat suppression is widely used in MR imaging for the elimination or detection/imaging of adipose tissue. In practice, three principal fat suppression techniques are available: fat saturation, inversion recovery, and opposed-phase imaging [2]. The selection of a method for fat suppression or water-fat imaging depends on the clinical application, and each such approach has its advantages and disadvantages resulting from its physical background. Generally, fat is bright in clinical images, and it may hamper the discernment of major pathologies such as tumour, edema, or inflammation; this problem is caused by a relatively short T_1 relaxation (240 to 280 ms [3]). Fat suppression methods, embedded into many clinical protocols, constitute an effective solution to the above-discussed issue, and the visualization of abnormalities in a normal tissue can thus be significantly improved [4]. One of the benefits of fat suppression consists in the elimination of chemical shift artefacts in clinical images. Together with direct visualization of fat, this can improve the detection of pathologies (such as fatty tumours and other fat-containing tumours), and it is possible to quantify and evaluate the amount of various kinds of adipose tissue [5], [6], [7], infiltrated fat in the tissue/organs in the case of fatty infiltrated liver diseases [8], [9], [10], [11], [12], or the amount of myocardial fat [13], [14], [15]. Many other clinical applications are also available (breast, knee, bone marrow [1], or optical nerves [16], [17]). If we understand the physical background of water-fat imaging methods, we can correctly estimate which method best suits our clinical application.

One of the most interesting domains in MRI consists in water and fat separation/suppression. The first articles describing various approaches for the separation/suppression of water and fat appeared almost 30 years ago. Methods for water and fat separation are based on two physical principles: longitudinal relaxation T_1 and chemical shift (CS). Each of the techniques exploits one of the above-mentioned principles, and all procedures developed for water and fat separation/suppression are utilized in clinical MR imaging (depending on the application and capabilities of the MRI system). The suppression/separation of water and fat is very useful in the treatment of fatty liver disease, and it also finds application in cardiology, magnetic resonance angiography (MRA), contrast-enhanced imaging, and other clinical processes or branches of medicine.

The most interesting group of water/fat separation techniques can be identified in Dixon methods; their principle is described in detail within Chapter 3. Dixon methods are very flexible and can be built into many imaging sequences; the range of clinical applications is practically unlimited. The magnetic field inhomogeneity owing to instability of the MR system or susceptibility influences is a major challenge for Dixon methods. Since the inception of these methods, research has been continually focused on finding the field inhomogeneity and reducing the measurement time.

2. Aim of the Thesis

In preclinical research, small animals are frequently used for the testing of drugs or animal models of diseases. Therefore, the use of a high field (4.7 T or more) is one of the techniques to increase the sensitivity. A high field nevertheless brings about specific problems, such as a stronger magnetic field inhomogeneity due to the differing susceptibility at the boundary between environments with diverse magnetic susceptibilities; on the other hand, it is also true that a high magnetic field leads to the high sensitivity, and the water-fat chemical shift is increased. The magnetic field inhomogeneity ($\mathbf{B}_0$) in Dixon-based methods causes problems during the reconstruction process, and the measurement must be as short as possible because the animal is anesthetized.

The aim of the thesis is to extend and implement modern MRI methods for water/fat separation and, consequently, to verify these techniques on phantoms and animal subjects at high fields (9.4 T) at the Institute of Scientific Instruments (ISI), Brno. The thesis assumes the modification or creation of a new fast Dixon sequence for water and fat separation; the implementation of the method on a 9.4 T MRI system; the verification on a phantom; and, finally, the eventual application in animals.

3. Dixon-Based Water-Fat Separation Methods

Dixon water-fat separation methods are chemical shift-based water-fat separation methods. Water protons precess faster between 3 and 4 ppm (the main fat peak) than fat protons, which results in different resonance water-fat frequencies. This difference is ≈ 1400 Hz at 9.4 T. The water-fat chemical shift, owing to different resonance frequencies between water and fat, leads to the water-fat phase shift. The discussed Dixon-based methods encode the water-fat chemical shift difference into the phase of the image, but water-fat separated images are obtained after the post-processing procedure.

In 1984, Thomas Dixon [18] introduced a new method for water-fat separation. This method already exploited differences in water and fat precession (Fig. 1(A)). If a 90° RF pulse is applied, the water and fat protons are flipped into the transversal plane. The total magnetization vector is the sum of water and fat magnetizations (Fig. 1(B)). The time behaviour of the transversal magnetization is shown in Fig. 1(C).

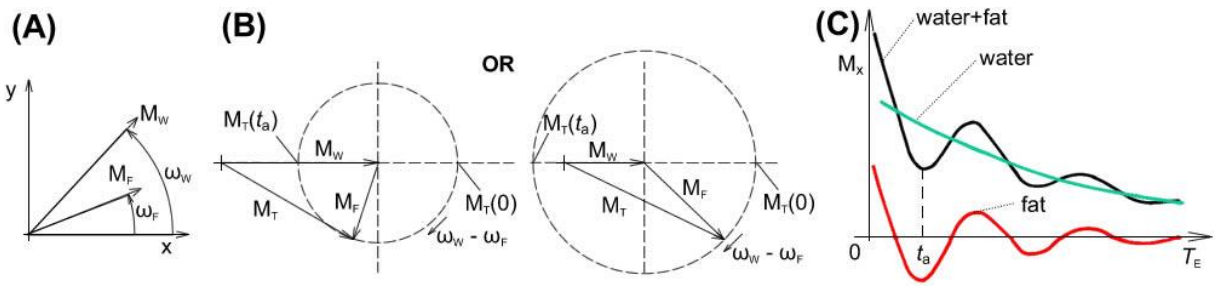

Fig. 1 (A) The laboratory frame. (B) The magnetization vectors of fat in a rotating frame, left $|M_W| > |M_F|$, right $|M_W| < |M_F|$. (C) The free induction decay (FID) signal. [18]

The total magnetization M_T is the sum of water and fat magnetizations. The rotating frame has the resonance frequency of water. The small differences in the resonance frequencies of water (f_W) and fat (f_F) lead to the rotation of fat in the rotating frame. At the beginning, $M_T(0)$, the water and fat are in phase. The magnetization goes through the first local minimum when fat and water are in opposite directions. The first local minimum occurs at [18]:

$$t = \frac{1}{2 \cdot (f_W - f_F)} = \frac{1}{2 \cdot (\Delta f_{CS})} \equiv t_a. \quad (1)$$

Another local maximum occurs at $2t_a$: water and fat then exhibit the same direction (in-phase). This time variation is periodical and depends on the different frequencies between water and fat. Simple summation or subtraction of the opposite-phase and the in-phase images is used to calculate a water-only or a fat-only image. Generally, this is a simple spectroscopic imaging concept.

The main problem of Dixon-based methods is the presence of a $\mathbf{B}_0$ inhomogeneity leading to phase errors in the acquired images. The phase errors in the in-phase and opposite-phase images result in incorrect water and fat separation; thus, phase correction is necessary for successful water-fat separation. Furthermore, Dixon methods require precise timing of the pulse sequence because the water/fat phase changes are relatively fast. At high fields (e.g., 9.4 T), the time between the in-phase (IF) and the opposite-phase (OP) images is much shorter compared to low fields (e.g., 1.5 T, 3 T). This fact follows from the above equation (1). The motion and incorrect pulse sequence timing cause the degradation of the obtained images [19].

In the past two decades, many Dixon-based water-fat decomposition methods have been proposed [20], [21], [22], [23], [24], [25], [26], [27], [28], [29], [30], [31], [32] to increase the robustness with respect to field inhomogeneity ($\mathbf{B}_0$ and $\mathbf{B}_1$). The problems affecting Dixon-based methods constitute a major topic, and multiple studies are focused on the correction of these drawbacks. Several procedures have been proposed to facilitate phase correction (post-processing algorithms, data acquisition, or a combination of both). Thus, the knowledge of the $\mathbf{B}_0$ inhomogeneity is crucial for correct water-fat separation. The phase correction and the data acquisition strategy are very significant for successful application of Dixon methods [19]. Significant development of Dixon-based methods has allowed their successful application in clinical MRI.

Dixon methods can be classified as single-point [33], two-point [24], [34], [35], [25], [28], [26], [36] and multipoint or triple ones [37], [21], [23], [29]; however, even higher variations are available [22], [38], [39], [40], [31]. The three or multipoint versions are preferred over the two-point variant when a short acquisition time is not required; in addition, they are more robust and enable more effective reconstruction of errors.

The signal model common for Dixon methods is represented by single delta function spectral peaks for water and fat. The signal model in the original 2PD method [18] was very simple and considered only two peaks (water and fat) without the presence of field inhomogeneity, system errors, and influences such as diffusion losses, intravoxel

susceptibility losses, or losses due to spectral broadening. Thus, other improvements were proposed for field inhomogeneity estimation [20], [21], [22], [27], [41], [42]. Generally, the signal model often assumes only the two-peak form (water and fat); however, multi-peak models were developed to provide for higher accuracy. A more accurate signal model results in significant improvement of the fat fraction estimation, and therefore the quantification of fat [10], [43], [42], [41] in a tissue or phantom is more accurate.

3.1 General Analysis

We assume the spectrum L(ω) with two spectral components, namely $L_1(\omega)$ (water) and $L_2(\omega)$ (fat), (Fig. 2(A)). The integrated real-value intensities of these lines can be denoted as ρ_1 and ρ_2.

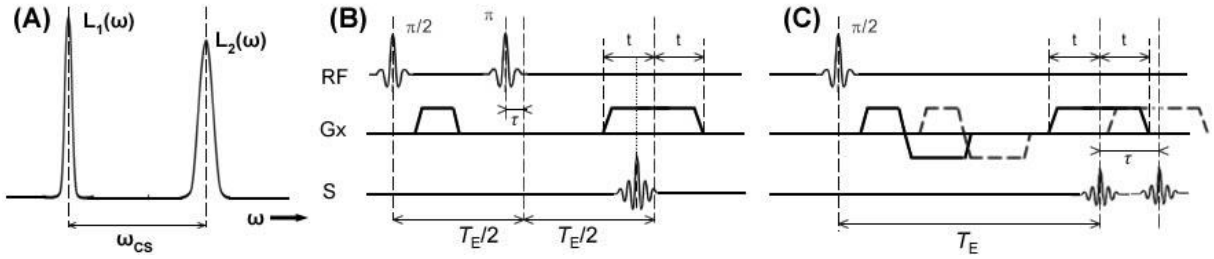

Fig. 2 (A) The simplified spectrum of water and fat protons. (B) The spin-echo sequence and (C) the gradient echo sequence for N-point Dixon methods. The images show only two-phase encoding positions - 2PD.

The multipoint Dixon method can be performed using the gradient-echo sequence (GRE) or the spin-echo sequence (SE) (Fig. 2(B) and (C)). In the GRE, we consider the following aspects: when the T_2 is very short and comparable with the echo time (T_E), then the losses owing to the T_2 decay must be taken into account. For our purpose, it is important to assume the condition $T_2 \gg T_E$. In this case or in the spin echo, the signal (S) acquired from one voxel in the time τ is a mixture of the water and fat components [22], namely

$$\begin{gathered} M_T = S_n(\tau) = \left(\rho_1 \cdot A_1(\tau) + \rho_2 \cdot A_2(\tau) e^{i\theta_n}\right) \cdot e^{i(\varphi+\varphi_0)}, \\ \rho_1 \cdot A_1(\tau) = M_W, \\ \rho_2 \cdot A_2(\tau) = M_F, \end{gathered} \tag{2}$$

where A_1 and A_2 are the loss factors for water and fat, which depend on the τ; θ is the phase difference between fat and water; φ represents the $\mathbf{B}_0$ field inhomogeneity (e.g., an imperfect shim and the influence of susceptibility); and φ_0 is the phase error due to system imperfections such as the different signal time delay in the receive channels, spatial dependence of the RF penetration [19], and other systematic phase shifts. The amplitudes of the loss factors A_1 and A_2 are affected by diffusion, susceptibility dephasing, and spectral broadening [22]. The total losses for water or fat can be calculated as follows:

$$A_m = A_{md} \cdot A_{ms} \cdot A_{mw}, \tag{3}$$

where m = 1, 2; A_d – the diffusion losses; A_s – the intravoxel susceptibility losses; and A_w – the losses due to spectral broadening. It follows from the above equation (1) that IP images

are acquired in zero time or even multiples of t_a, and OP images are acquired in odd multiples of t_a. Generally, the phase difference θ is proportional to τ, that is

$$\theta[\text{rad}] = 2\pi \cdot \gamma \cdot \mathbf{B}_0 \cdot \Delta\delta[\text{ppm}] \cdot 10^{-6} \cdot \tau = 2\pi \cdot \Delta f_{\text{CS}} \cdot \tau. \quad (4)$$

The phase error is too proportional to τ, and we have

$$\varphi = 2\pi \cdot \Delta\mathbf{B}_0 \cdot \tau, \quad (5)$$

where $\Delta\mathbf{B}_0$ is the magnitude of the field inhomogeneity.

4. Fast Triple-Spin Echo Dixon Method (FTSED)

The Fast Triple-Spin Echo Dixon Sequence (FTSED) is derived from the conventional fast spin echo (FSE) method proposed by Hennig et al. [44] and can be classified as a 3PD method. The main goal of the proposed method (FTSED) lies in the acquisition of three independent k-spaces, each for a specific echo shift (Fig. 4), during one instance of FTSED acquisition; thus, the Dixon acquisition time will be equal to the FSE method duration. Fig. 4 shows a FTSED sequence for particular phase encoding steps (0, -π, -2π). Generally, however, the echo shifts can be chosen arbitrarily (within the limits of the sequence), and the Iterative Least-Squares Estimation Method [38] can be used for water and fat calculation. Reeder et al. [29] indicate that symmetrically acquired echoes cause artefacts which degrade image quality; therefore, symmetrical phase encoding strategies were excluded a priori. In addition, the authors found an optimal echo combination where noise performance reaches the achievable maximum and will be independent from the proportion of water and fat. The combination of asymmetrically acquired echoes with the Iterative Least-Squares Estimation is referred to as "iterative decomposition of water and fat with echo asymmetry", IDEAL [29]. In our case, the specific asymmetric phase encoding strategy was chosen: (0, -π, -2π) or (0, π, 2π). The chosen strategy will ensure the achievement of PD –, T_2^* –, T_2 – weighted images (e.g., Fig. 12 (A), (B), (C)).

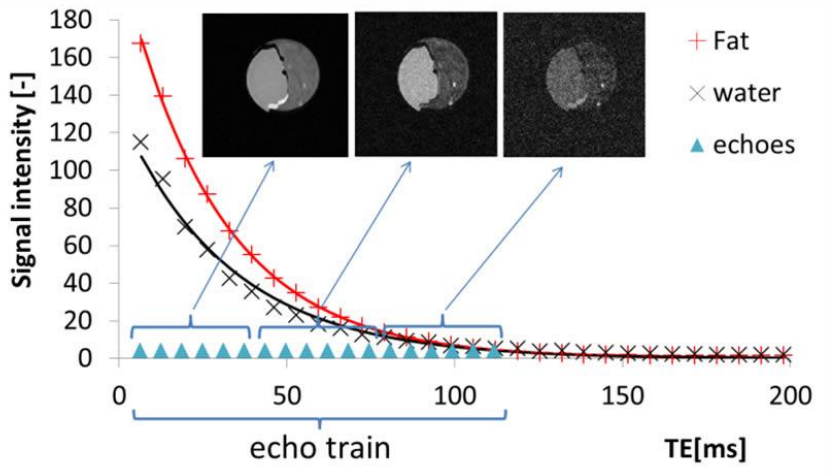

Fig. 3 The course of water and fat T_2 relaxation in the phantom (water and fat/lard) during the FTSED sequence.

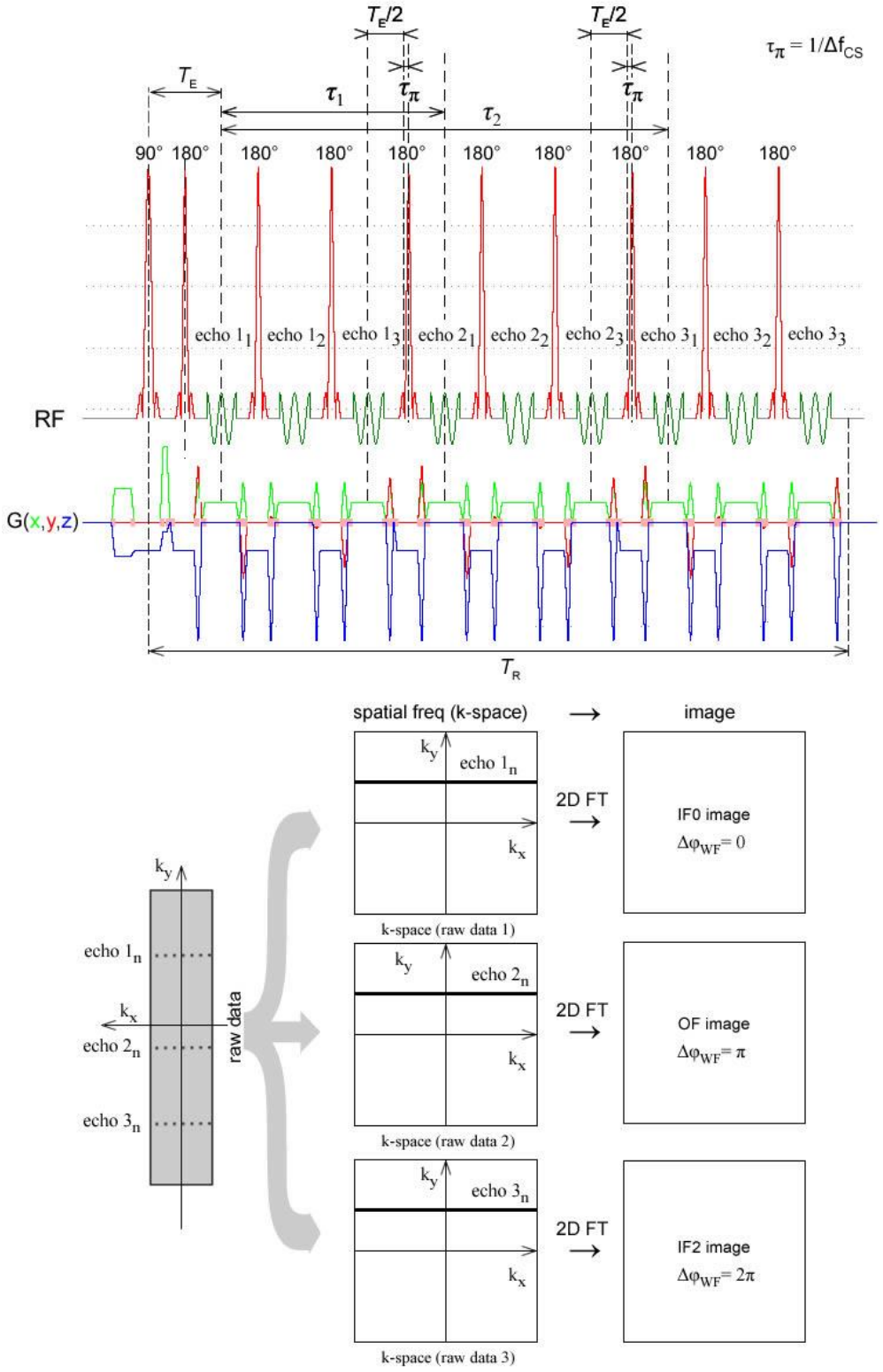

Fig. 4 The time diagram of the Fast Triple Spin Echo pulse sequence for a particular phase encoding scheme, or 0, π, 2π, and the principle of data acquisition; ETL = 9, FTSED-factor = 3. Three images are obtained during a single acquisition: an in-phase image (IF0), an opposite-Phase image (OP), and an in-phase image (IF2) again, but with the phase difference between water and fat of 2π. n = FTSED-factor = 3.

The principle of the FTSED lies in the insertion of three (or two) time intervals into the echo train (ET); thus, the three images, each with a specific phase shift between water and

fat, are obtained during one FTSED acquisition. This manner of acquisition nevertheless comprises one disadvantage, namely the ETL limitation compared to other FSE-based sequences, e.g. the fTED or asymmetric FSE (AFSE). In fact, the ETL is limited only by the T_2 relaxation of the measured sample/tissue (Fig. 3).

It is necessary to mention that the ETL in the FTSED method carries the same meaning as in the FSE echo method, yet there is a little difference: the ETL in the FSE sequence means the number of echoes in the echo train and the acceleration factor. In the case of the FTSED sequence, the ETL defines only the number of refocused echoes in the echo train, and the acceleration FTSED-factor is equal to the ETL/3. The method enables us to choose an arbitrary phase-encoding strategy and generally depends only on our choice. To achieve a stronger contrast between a voxel with dominant water and voxels where fat is dominant, the modified IDEAL algorithm can be used.

5. Results

The proposed method was successfully implemented in an 9.4 T MRI system (Bruker, BioSpec 94/30). Two phantoms were created for the evaluation of the FTSED method, the first being a set of plastic tubes (twelve) containing a water-fat emulsion (mayonnaise mixed with water), each with various water/fat ratios. The second phantom consisted in a compound of lard and water placed into a glass tube. Consequently, the method was applied in rats. All animal measurements were performed with real-time breath-hold triggering (SAII, Model 1030), and each measurement followed in the pause (or interval) after exhalation. All calculations were performed in the Matlab program.

The first phantom (Fig. 6) with various concentrations of fat in water was created upon the necessity to verify correct determination of the fat fraction (FF).The fat signal fraction can be calculated as follows [45]:

$$FF = \frac{|F|}{|F| + |W|}, \tag{6}$$

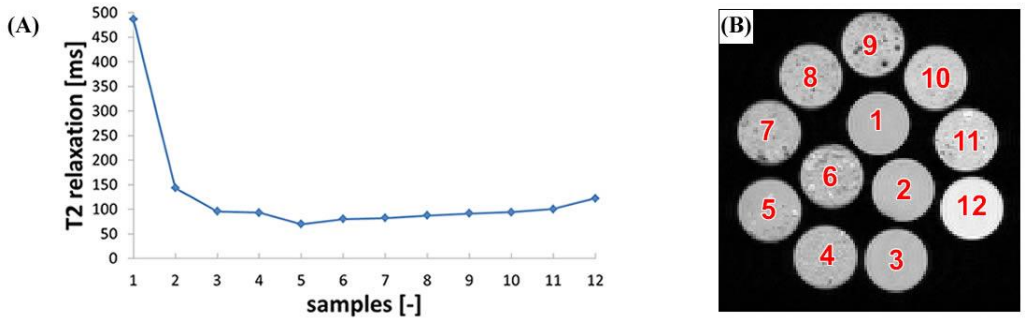

Fig. 5 The calculated transversal relaxations T_2 of samples in the phantom, (A). The numerical designation of samples in the phantom, (B).

The spiral displacement of the tubes in the phantom can be seen in Fig. 5B. Each sample exhibits its own T_2 relaxation (Fig. 5A). The spectrum of the whole phantom is

presented in Fig. 9(A). To improve the stability of the emulsion, the water was mixed with gelatine before being blended with mayonnaise. The mayonnaise was created only from chicken egg and sunflower oil. The mixing of water and oil is a problematic task if performed without an emulsifier. An emulsifier is a substance which reduces the surface tension at the interface between two immiscible liquids, thus enabling homogeneous mixing of the emulsion of the two liquids. In our case, the lecithin in a chicken egg was utilized as a natural emulsifier.

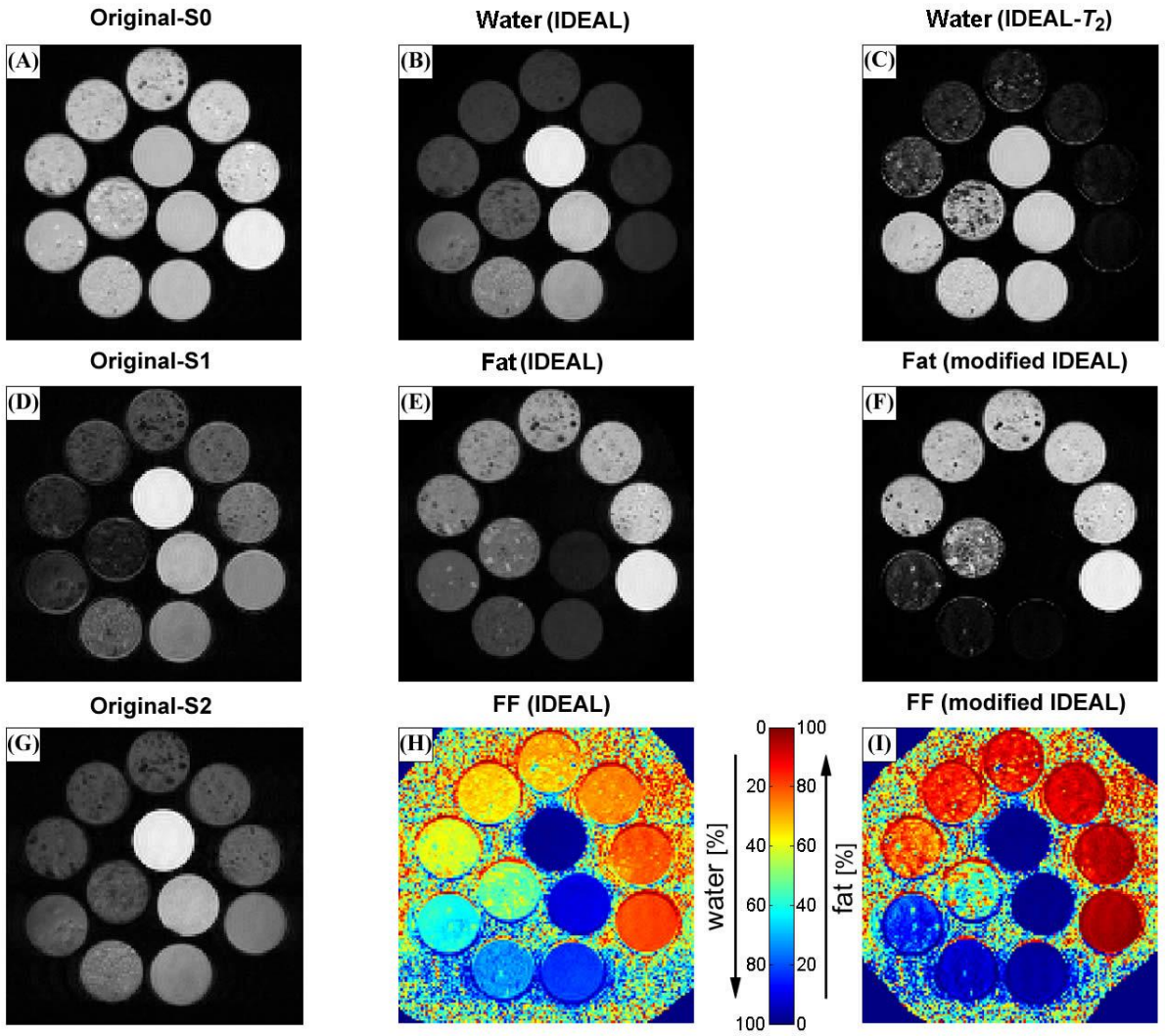

Fig. 6 The phantom with various ratios of water and fat. (A), (D, (G) are the original images used for the calculation of water and fat images through the use of the IDEAL (B), (E) and the modified IDEAL (C), F) algorithms. The fat fraction calculated for the IDEAL, (H) and the modified IDEAL, (I). The sequence parameters: ETL = 12, (FTSED - factor = 4), BW = 150 kHz, T_R = 3000 ms, T_E = 4.774 ms, ETE(S_0) = 9.548 ms, ETE(S_1) = 28.955 ms, ETE(S_2) = 48.362 ms, matrix = 128 x 128, FOV = 60 x 60 mm; total scan time = 1 m 36 s.

The graph in Fig. 7 shows the values of FF calculated through the use of the IDEAL and the modified IDEAL algorithms for various concentrations of fat. The ROIs were selected over each sample. The red line indicates the theoretical concentration of fat in the emulsion. However, not all samples in the phantom were homogeneous, and therefore the calculated FF maps vary from the theoretical concentration, especially for samples 5 – 7 and 9 – 10. In

addition, the emerging small air bubbles exert an undesirable effect on the calculated FF from the ROIs. The dashed lines with filled circles show the FF calculated via the IDEAL algorithm. The contrast between the voxels with dominant water or fat can be improved (modified IDEAL), but the resulted FF image is not correct. The solid black lines (Fig. 7) with triangles show that the signal is suppressed in voxels with dominant water and boosted in the fat-dominated voxels. The result is a higher contrast between water and fat. The same findings can be mentioned for water images. The difference between the calculated FF achieved via the FTSED-IDEAL and the theoretical FF (the red solid line) is shown in Fig. 8. In the samples 9 – 12, we evaluated the FF (the blue solid line) acquired from chemical shift imaging (CSI). The FF values were calculated for the same ROIs as in the case of FTSED.

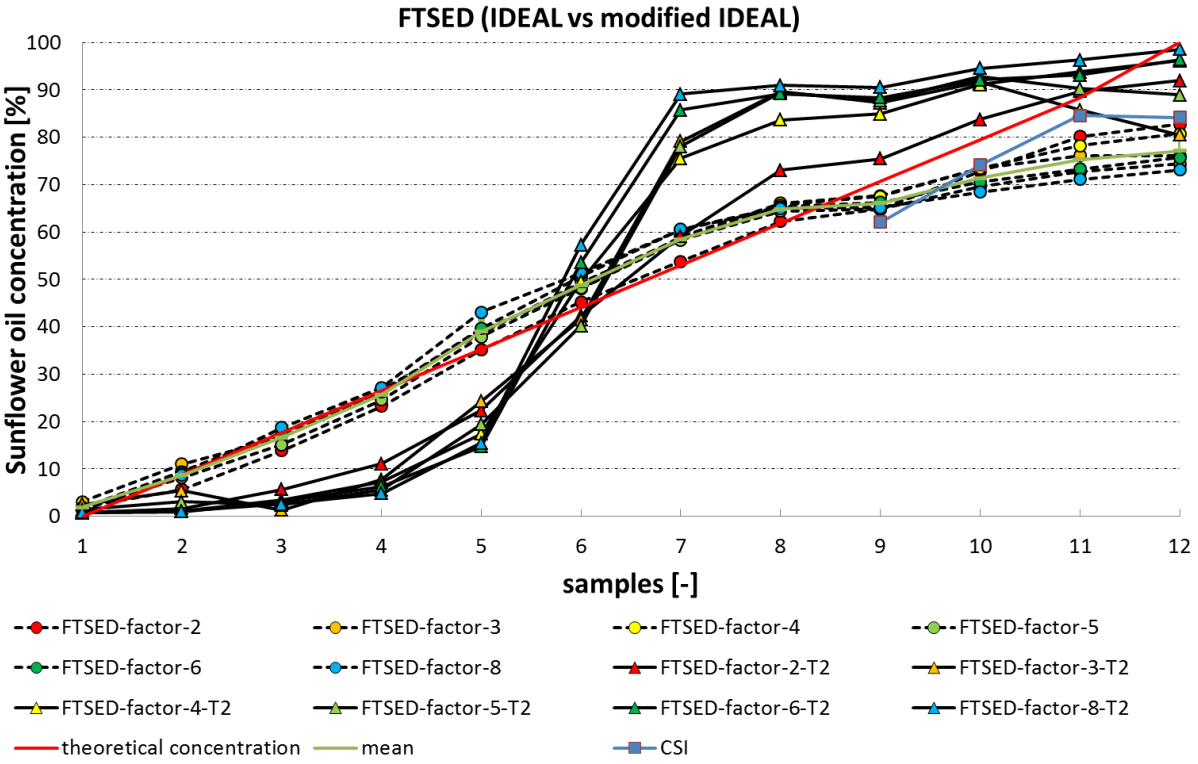

Fig. 7 The theoretical concentration of fat in the emulsion (solid red line) compared to the measured data. The fat fraction was calculated via the IDEAL (filled circles with dashed lines) and the modified IDEAL (filled triangles with solid lines) algorithms.

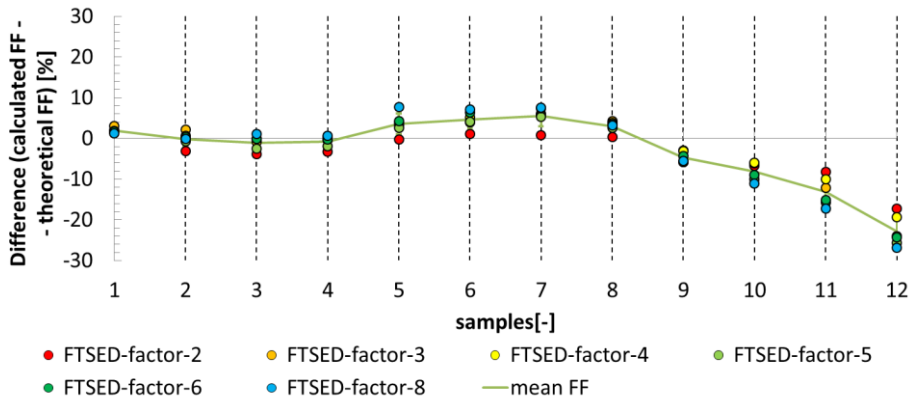

Fig. 8 The graph showing the level of agreement between the theoretical and the calculated FF (IDEAL).

Fig. 10 – Fig. 13 show the original images (A), (B) and (C) of the second phantom and a rat acquired by the FTSED method; (D), **(**E) and (F) are the corresponding phase images. The images were used for the calculation of water and fat images through the use of the IDEAL (H and I) and the modified IDEAL ((K) and (L)) algorithms. From the calculated water and fat images, images were recombined for the IDEAL (G) and the modified IDEAL (J). The images (A), (B) and (C), for the selected phase encoding strategy (0, π, 2π), represent PD –, T_2^*– and T_2 – weighted images.

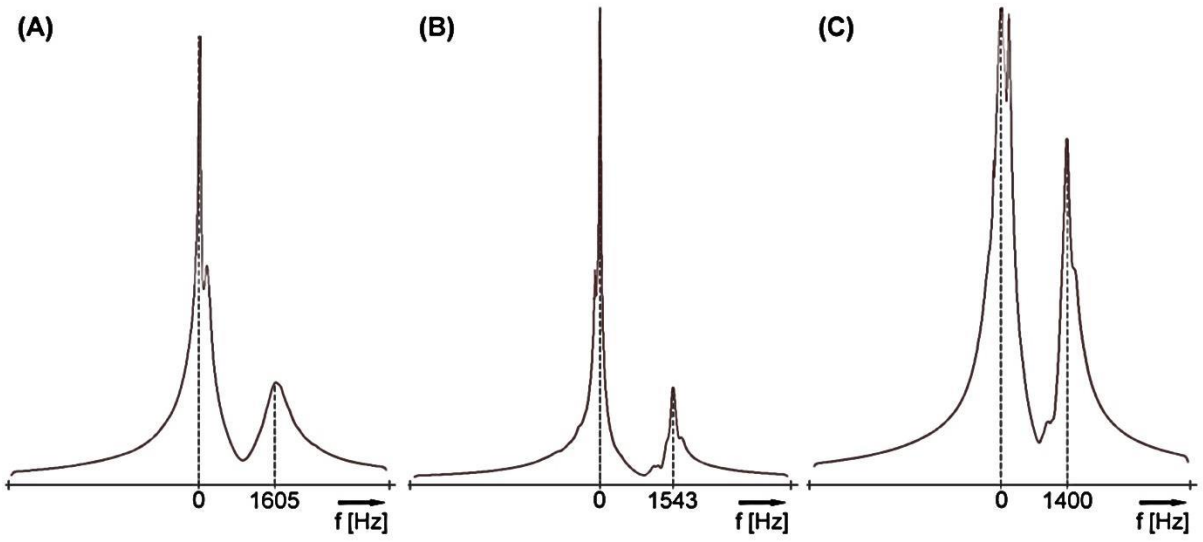

Fig. 9 The spectra of the measured phantoms (A – water-oil emulsion; B – lard and water) and a rat (C) acquired at 9.4 T. BW = 8kHz, 2048 points.

Fig. 10 and Fig. 11 show axial slices of the measured phantom compound from the water (T_1 = 56.5 ms, T_2 = 29.1 ms) and fat-lard (T_1 = 508.3 ms, T_2 = 33.4 ms) placed into the applied glass tube. The chemical shift between water and fat is 1543Hz (Fig. 9(B)). The effects of a relatively long ETL and a "short" T_2 lead to errors in the reconstructed water and fat images (Fig. 11 (J), (K), (L). The errors in reconstruction occur due to a lower SNR in the images used for the reconstruction. A lower frequency bandwidth (BW) leads to a higher SNR, but, on the other hand, a low BW yields a bigger shift between water and fat in the image. The effect of a low BW at a high field can be seen in Fig. 11; the water-fat shift is 1.2344 mm in the reading direction. This regrettable effect can be partially eliminated by the exchange of the BW for the same FOV. The position shift between water and fat in the image for a higher BW is shown in Fig. 10. In this case, the shift is only 0.3086 mm. Generally, the shift between water and fat Δx in the image can be expressed as

$$\Delta x = \frac{FOV}{BW} * \Delta f_{CS} \tag{7}$$

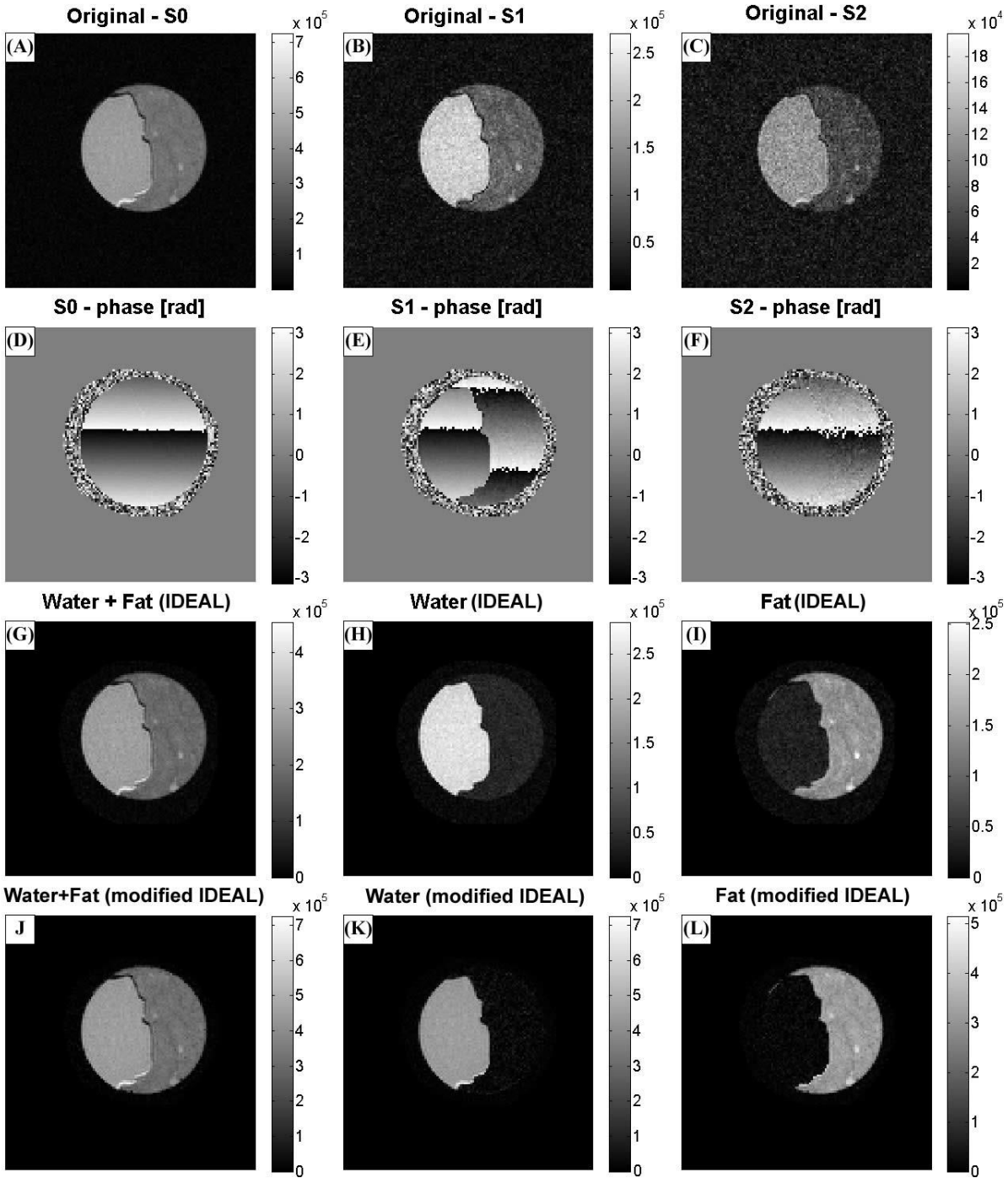

Fig. 10 A comparison of the IDEAL and the modified IDEAL algorithms for water and fat separation. Axial images of the phantom (water and fat/lard in a glass tube) were acquired using the FTSED sequence (0, π, 2π). The images (A) – **(**C) show the magnitudes (intensities), and (D) – **(**F) are the corresponding phase images. The calculated water and fat images (H), (I) utilizing the IDEAL algorithm, and the recombined image (G). The images (K) and (L) represent the calculated water and fat images using the modified IDEAL, and the following image **(**J**)** is an image recombined from the previously mentioned ones. Sequence parameters: ETL = 9, (FTSED - factor = 3), BW = 200 kHz, T_R = 2000 ms, T_E = 6.206 ms, ETE(S_0) = 12.412 ms, ETE(S_1) = 31.387 ms, ETE(S_2) = 50.362 ms, matrix = 128 x 128, FOV = 40 x 40 mm; total scan time = 1 m 24 s.

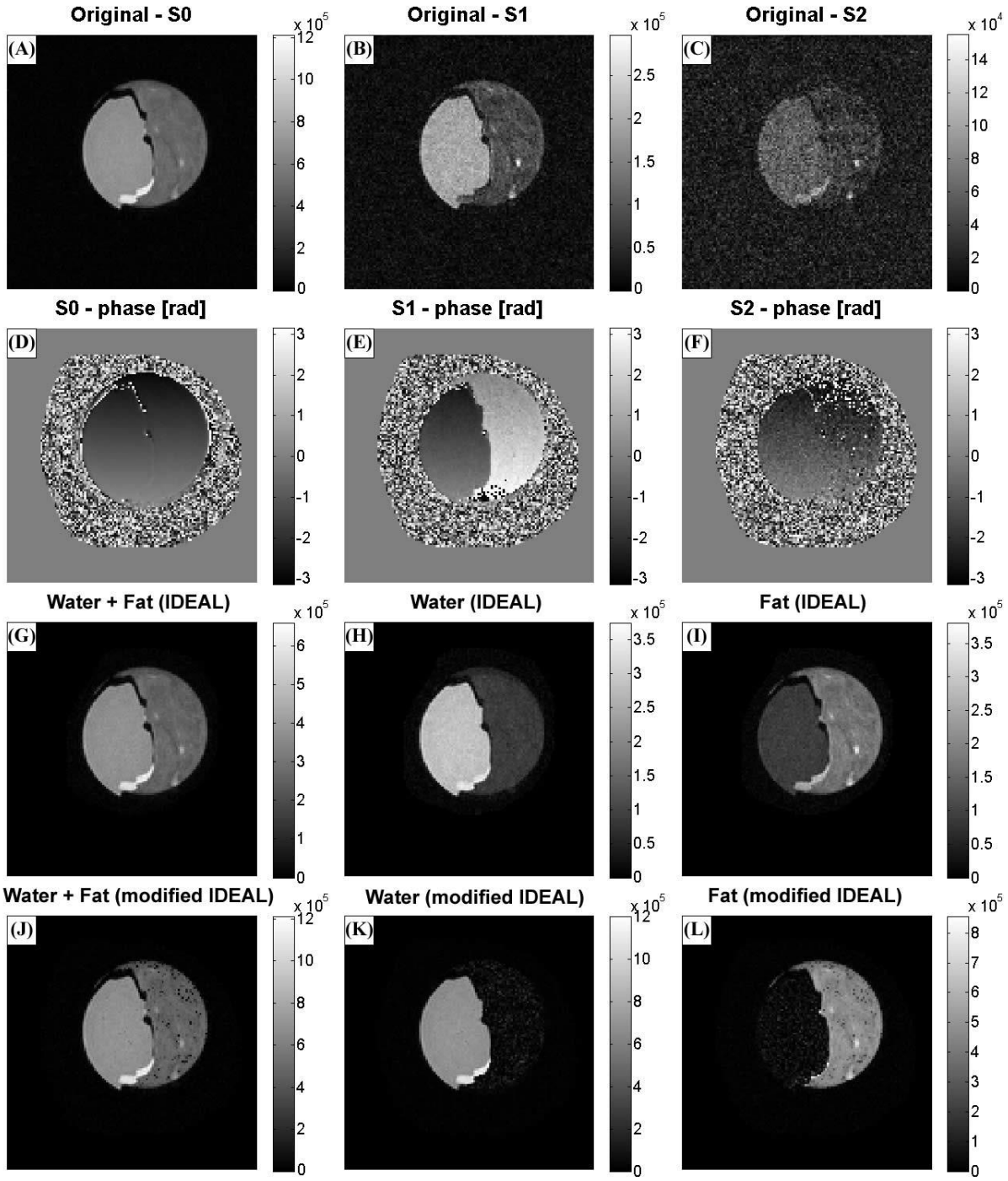

Fig. 11 A comparison of the IDEAL and the modified IDEAL algorithms for water and fat separation. Axial images of the phantom (water and fat/lard in a glass tube) were acquired using the FTSED sequence (0, π, 2π). The images (A) – (C) show the magnitudes (intensities), and (D) – (F) are the corresponding phase images. The calculated water and fat images (H), (I) utilizing the IDEAL algorithm, and the recombined image (G). The images (K), (L) represent the calculated water and fat images using the modified IDEAL, and the following image (J) is an image recombined from the previously mentioned ones. The sequence parameters: ETL = 18, (FTSED - factor = 6), BW = 50 kHz, T_R = 2000 ms, T_E = 6.206 ms, ETE(S_0) = 18.618 ms, ETE(S_1) = 56.211 ms, ETE(S_2) = 93.804 ms, matrix = 128 x 128, FOV = 40 x 40 mm; total scan time = 42 s.

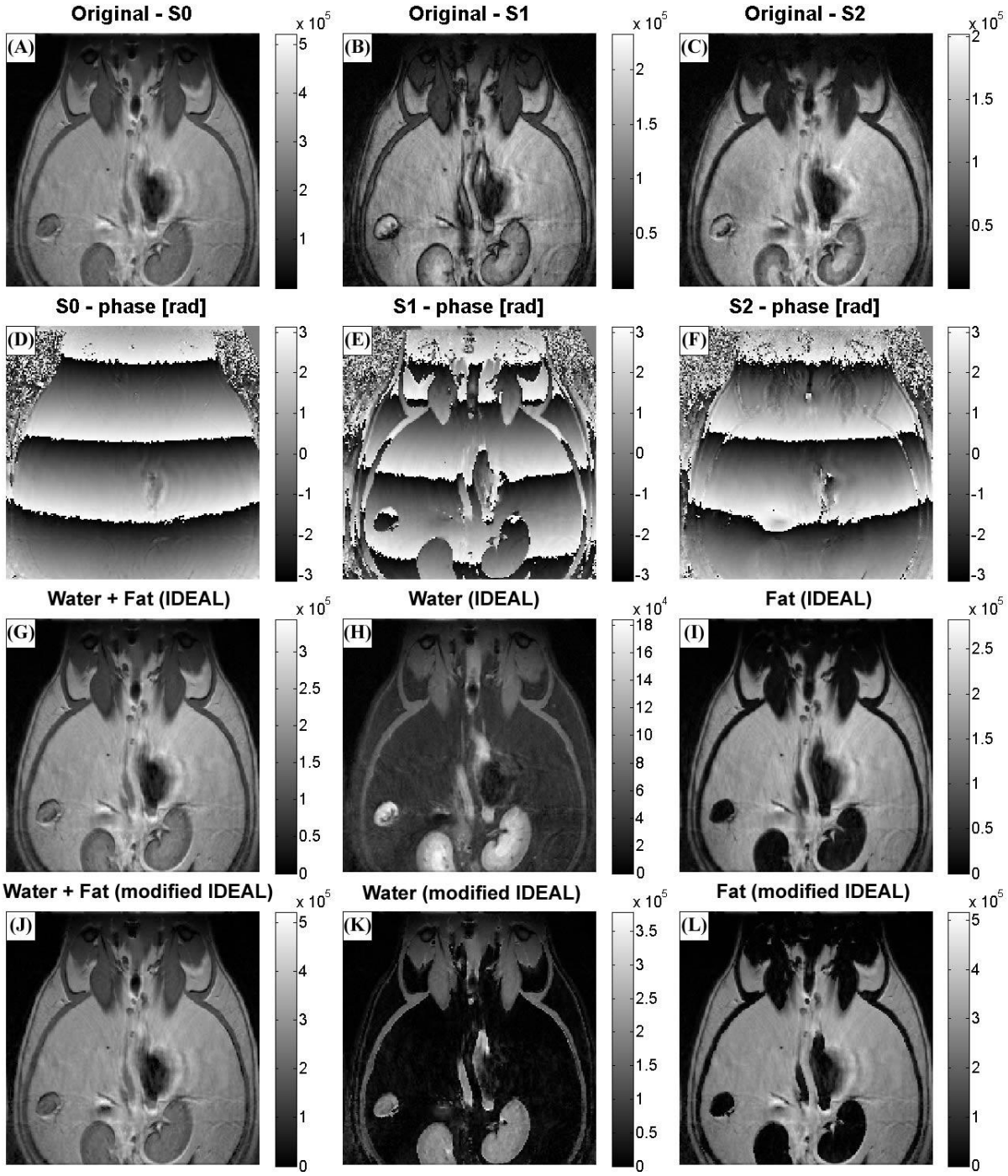

Fig. 12 A comparison of the IDEAL and the modified IDEAL algorithms for water and fat separation in rats. The coronal images of a rat (abdomen and pelvic region) were acquired using the FTSED sequence (0, π, 2π). The images (A**)** – **(**C**)** show the magnitudes (intensities), and (D) – **(**F**)** are the corresponding phase images. The calculated water and fat images (H), (I) utilizing the IDEAL, and the image recombined from the previously mentioned ones (G). The images (K) and (L) represent the calculated water and fat images using the modified IDEAL, and the following image **(**J**)** is a recombined image. Sequence parameters: ETL = 12, (FTSED - factor = 4), BW = 150 kHz, T_R = 3000 ms, T_E = 4.774 ms, ETE(S_0) = 9.548 ms, ETE(S_1) = 29.001 ms, ETE(S_2) = 48.454 ms, matrix = 192 x 192, FOV = 70 x 70 mm; total scan time = 2 m 24 s.

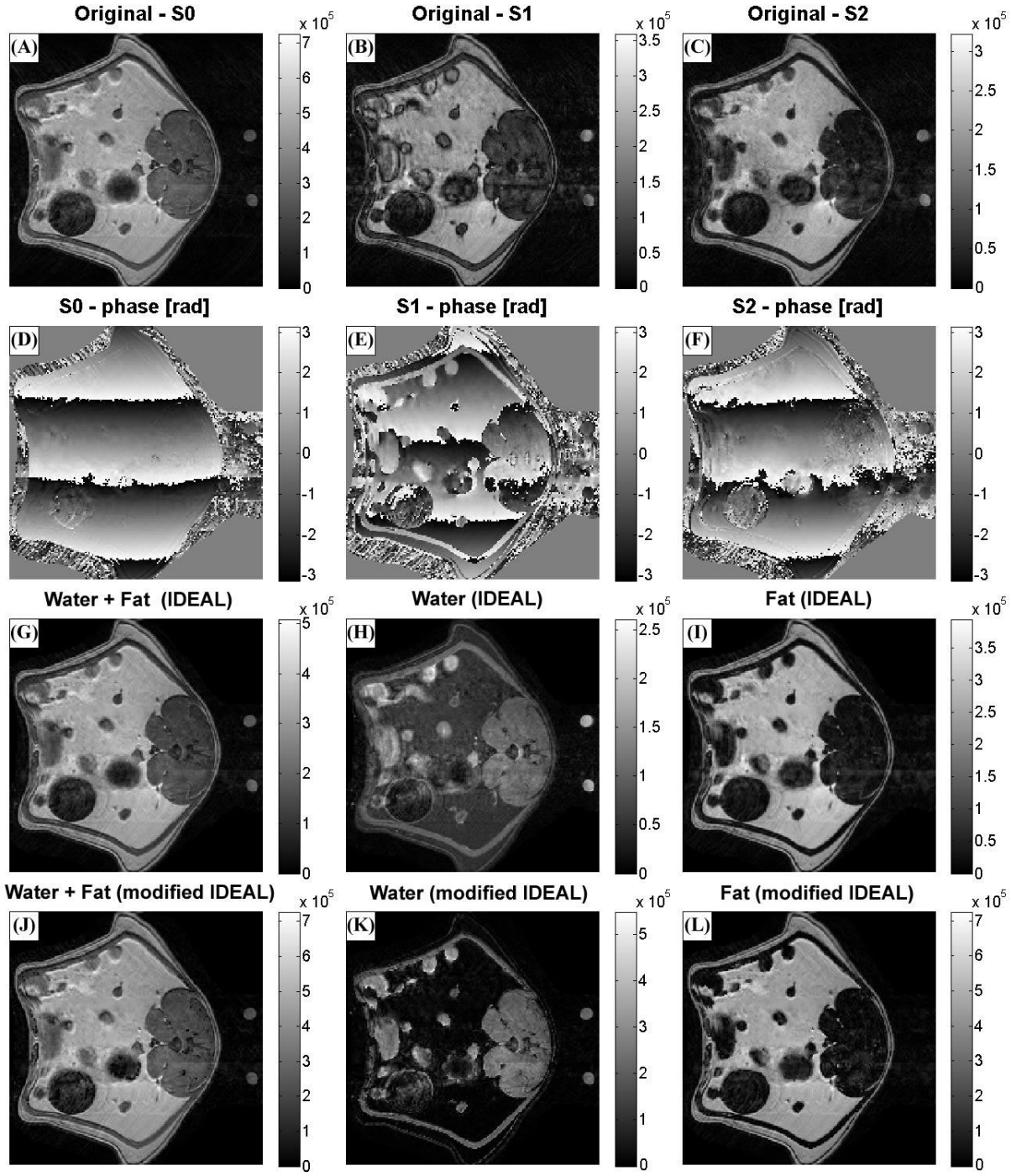

Fig. 13 A comparison of IDEAL and the modified IDEAL algorithms for water and fat separation in rats. The transversal images of a rat abdomen were acquired using the FTSED sequence (0, π, 2π). The images (A**)** – **(**C**)** show the magnitudes (intensities,) and (D**)** – **(**F**)** are the corresponding phase images. The calculated water and fat images (H**)**, (I) utilizing the IDEAL, and the image recombined from the previously mentioned ones (G). The images (K) and (L) represent the calculated water and fat images using the modified IDEAL, and the following image **(**J**)** is a recombined image. The sequence parameters: ETL = 12, (FTSED – factor = 4), BW = 150 kHz, T_R = 3000 ms, T_E = 4.774 ms, ETE(S_0) = 9.548 ms, ETE(S_1) = 29.001 ms, ETE(S_2) = 48.454 ms, matrix = 192 x 192, FOV = 70 x 70 mm; total scan time = 2 m 24 s.

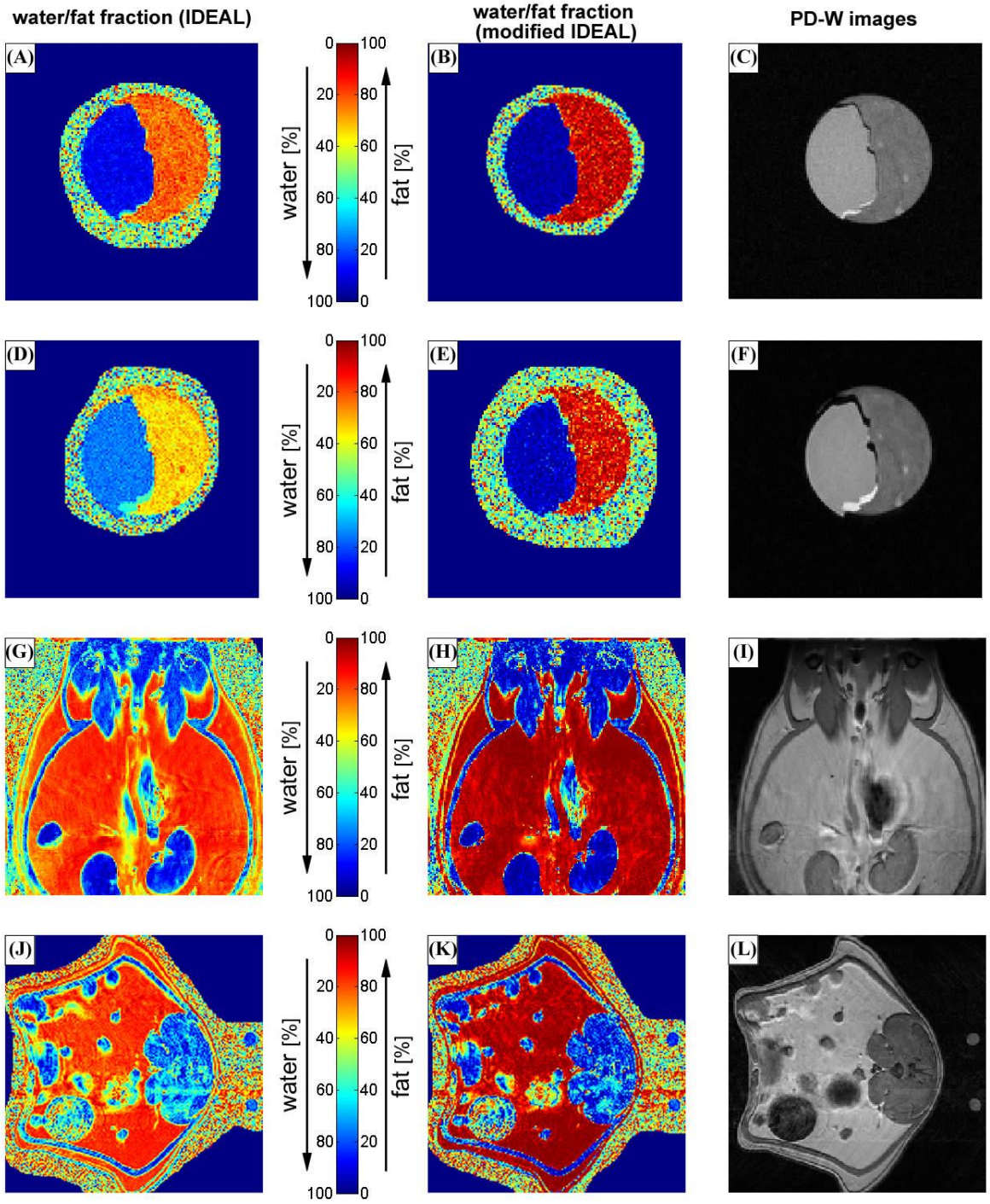

Fig. 14 The calculated water/fat fraction images for the phantom and the rat abdomen/pelvic region. The water/fat images calculated from the images achieved from the IDEAL, (A), (D), (G), (J), and the modified IDEAL (B), (E), (H), (K) algorithm.

After the verification of the FTSED method in both phantoms, the method was applied in a rat. Fig. 12 shows the coronal slice of a rat abdomen with the pelvic region. Although the measurement was triggered, the images are slightly affected by motion artefacts because the respiration rate was not absolutely stable during the entire measurement. Fig. 13 shows transversal slices through the rat abdomen, where the motion artefacts are stronger. The artefacts are mainly visible in the phase images (D) - (F). The artefacts arise owing to the peristaltic movement of the gastrointestinal tract (intestines and stomach); thus, the abdominal

fat around the gastrointestinal tract is affected by motion too. It can be clearly seen in the water and fat images (H**)**, (I**)**, (K**)**, (L) that the artefacts are primarily due to the fat or water.

Fig. 14 shows the calculated FF and WF for the phantom and the rat abdomen/pelvic region. The spurious effect of the motion artefacts can be seen mainly in the axial slice of rat abdomen (J), (K), and a minor effect of motion artefacts can be observed in the coronal slice of the rat abdomen/pelvic region (H), (I). A strong motion artefact leads to errors in the determination of the correct fat/water fraction. The calculated water/fat fraction (B), (E**)**, (H), (K) images, from the water and fat images achieved by the modified IDEAL algorithm, show different results compared to the original IDEAL algorithm (A**)**, (D**)**, (G**)**, (J) – true value of the FF.

6. Discussion

The novel 3PD fast triple spin echo Dixon method (FTSED) is introduced. The proposed technique, derived from the original fast spin echo (FSE) with echo asymmetry, was successfully implemented in an 9.4T MRI system. The measurement at a high field is accompanied by specific problems, which include the consequences of the magnetic susceptibility inhomogeneity: considerable local static field inhomogeneity may lead (in some voxels) to significant resonance line broadening, which then may complicate the separation of the water and fat components. The T_2 transversal relaxation shortening at a high field constrains the proposed method. The 3PD method assumes a relatively simple signal model where water and fat have a single resonance frequency, in spite of the fact that fat exhibits several spectral peaks.

The main goal of the FTSED method lies in the acquisition of 3 raw data sets (each with a specific water-fat phase shift) during one scan and in the provision of images with a high SNR. In comparison with the 3PD realized via the FSE with echo asymmetry, sometimes denoted as the AFSE, the total scan time of the FTSED is 3 times shorter. The FTSED method is directly a 3PD method. In addition, the selected phase-encoding scheme (0, π and 2π) provides three different image contrasts (PD, T_2*, and T_2-weighted images), as shown in Fig. 12 (A), (B), (C). The time efficiency is directly comparable to that found in another modification of the FSE method: the fast spin-echo triple-echo Dixon (fTED) technique [149]. From the perspective of image processing, the fTED is a 2PD method.

At high fields, the chemical shift between water and fat is increased, and to minimize chemical shift artefacts, strong gradients and a large acquisition bandwidth must be used, in which the set of possible consequences includes non-negligible eddy currents or a reduced SNR. The choice of a low acquisition BW leads to non-negligible chemical shift artefacts in the image. The effect of a low BW is shown in a phantom (Fig. 11). In this case, the gradients of ~29mT/m were insufficient because the chemical shift displacement is 1.23 mm, with the pixel size of 0.31 mm, and it represents a 4-pixel displacement. As can be seen in Fig. 10, the higher acquisition BW reduced the chemical shift displacement. In this case, the gradients of ~117mT/m were sufficient to limit the chemical shift displacement to ~0.31 mm, and this

shift represents only a 1-pixel displacement. On the other hand, the SNR reduction in the image is apparent. A high field causes shortening of the T_2 relaxation time; thus, the combination of a very long echo train and a short T_2 relaxation (Fig. 16 and Fig. 24) leads to errors in the calculated water and fat images, and the computed FF maps will be wrong (Fig. 14 (D)).

A phantom with various fat concentrations was created for the verification of the FTSED method. Unfortunately, the concentrations determined from the FTSED – IDEAL differ from the expected values (Fig. 7, red solid line) for several reasons, including the inhomogeneity of the water-fat emulsion, the simplified signal model, and the field inhomogeneity (T_2*). Over all these effects, the FTSED method with IDEAL exhibits the ability to determine the FF fraction relatively accurately. The FF determined upon the FTSED – IDEAL for samples 10 – 12 significantly differs from the expected (theoretical) values, but the FFs obtained from the chemical shift imaging (CSI) method are closer to the FF achieved with the FTSED – IDEAL. It follows from this assertion that vegetable oil comprises an inconsiderable amount of water, and this is inconsistent with our original assumption of pure oil. The second phantom (Fig. 10 and Fig. 11) was created from lard and water. Lard is an animal fat whose properties are similar to those of fat in a live animal. The water-fat calculation was successful, but in the case of a relatively long ETL compared to short T_2 relaxations (Fig. 24) the reconstruction can produce misleading water/fat images and FF maps.

The contrast between water- and fat-dominant voxels can be increased via the modified IDEAL. This is indicated in Fig. 7, where the full triangles with solid black lines represent data calculated through the use of the modified IDEAL algorithm. In the image of fat, signals from the fat-dominated pixels are boosted, while signals from the water-dominated pixels are suppressed. In the case of an equal amount of fat and water in the voxel, the signal in the voxel remains unchanged. The acquired images can be useful, similarly to other contrasts for multiparametric segmentation. The calculated FF maps acquired from the modified IDEAL algorithm do not provide true values.

Compared to the measurement of human patients, the monitoring of small animals brings about specific problems; most importantly, the animal must be anesthetized before each measuring step (+ life functions scanning), and all measurement of the abdomen or heart must be triggered (synchronized). It is vital to note that the metabolism of small animals (e.g., rabbits, rats, mice) is much faster than that of humans or big animals; generally, however, the respiration and heart rate is lower under anesthesia. The heart and respiration rate [172] differs between individual animals. If correct synchronization is not ensured, the motion artefacts can be very strong or the measurement may fail. The coronal (Fig. 12 (A) – (C)) and axial images (Fig. 13(A) – (C)) acquired by the FTSED sequence were processed by the IDEAL and modified IDEAL algorithms. The rat coronal slice is not motion artefacts-free, but in this case such artefacts are still acceptable. The rat axial slices are strongly affected by motion artefacts because the movement is stronger in the given direction. The undesirable effect of motion artefacts can be observed in the original and calculated water/fat images and, mainly, in the FF map (Fig. 14 (J)). Although the motion artefacts cannot be removed

completely, they can be reduced through the use of non-Cartesian k-space sampling (e.g., PROPELLER [173] [174]) in the method.

The fast triple-spin echo Dixon (FTSED) sequence applied in this thesis represents a novel, efficient, T_2-weighted Dixon imaging method, and it ensures good water/fat separation when combined with iterative decomposition of water and fat, echo asymmetry, and the least-squares estimation (IDEAL) algorithm. The method enables us to acquire 3 raw-data images during one acquisition, and the acquisition time is equal to the original FSE sequence. The method is extremely time-efficient. The time efficiency is comparable to another T_2-weighted method, namely the fast spin-echo triple-echo Dixon (fTED) method presented by Ma et al. [149]. In the FTSED method, the time shifts are changed directly, but in the fTED method the positions of the echoes (the phase encoding strategy) are changed through the BW. A high field means a greater echo shift; thus, the echo shift is much shorter than at a low field. This can be problem for the fTED method, where the echo shifts are controlled through the change of the BW, and the time echo shift is practically limited by the gradient ramp time (to achieve a 180° water-fat phase difference is very problematic). In the case of the FTSED method, the minimal echo shift is practically unlimited. Unlike the fTED method, the FTSED technique using the asymmetric phase encoding strategy (0, π, 2π) appears to be more advantageous than that exploiting the symmetrical encoding strategy ($-\pi$, 0, π).

7. Conclusion

A new modification of a specific Dixon method was proposed and verified on phantoms and animal subjects. The method was successfully implemented using a 9.4T MRI (Bruker) system at the Institute of Scientific Instruments, ASCR Brno. The fast triple spin echo Dixon (FTSED) sequence is a 3PD time-efficient, T_2-weighted method, where 3 images are acquired simultaneously and used for the calculation of water and fat images. Therefore, the method is three time faster in comparison with the asymmetric fast spin echo (AFSE) three-point Dixon (3PD) method. The duration of the FTSED sequence is comparable to the original FSE sequence, and the FTSED method is a single-scan, T_2-weighted method providing three images simultaneously. Furthermore, the specific phase-encoding strategy (0, π, 2π) provides three different contrasts (PD, T_2*, T_2). The method constitutes a viable perspective for preclinical and clinical MR imaging. Successful implementation of the method at a high-field MRI system points to the possibility of the technique being used on a low-field MRI system.

8. List of References

[1] J. M. Patsch, X. Li, T. Baum, S. P. Yap, D. C. Karampinos, A. V. Schwartz and T. M. Link, "Bone marrow fat composition as a novel imaging biomarker in postmenopausal women with prevalent fragility fractures.," *J Bone Miner Res,* vol. 28(8), pp. 1721-1728, August 2013.

[2] E. M. Delfaut, J. Beltran, G. Johnson, J. Rousseau, X. Marchandise and A. Cotten, "Fat suppression in MR imaging: techniques and pitfalls.," *Radiographics,* vol. 19(2), pp. 373-382, March-April 1999.

[3] G. Hamilton, D. L. J. Smith, M. Bydder, K. S. Nayak and H. H. Hu, "MR properties of brown and white adipose tissues.," *J Magn Reson Imaging,* vol. 34(2), pp. 468-473, Aug 2011.

[4] T. A. Bley, O. Wieben, C. J. François, J. H. Brittain and S. B. Reeder, "Fat and water magnetic resonance imaging.," *J Magn Reson Imaging,* vol. 31(1), pp. 4-18, January 2010.

[5] X. Li, J. Youngren, B. Hyun, G. Sakkas, K. Mulligan, S. Majumdar, U. Masharani, M. Schambelan and I. Goldfine, "Technical evaluation of in vivo abdominal fat and IMCL quantification using MRI and MRSI at 3 T.," *Magn Reson Imaging,* vol. 26(2), pp. 188-197, February 2008.

[6] D. Armao, J. Guyon, Z. Firat, M. Brown and R. Semelka, "Accurate quantification of visceral adipose tissue (VAT) using water-saturation MRI and computer segmentation: preliminary results.," *J Magn Reson Imaging,* vol. 23(5), pp. 736-741, May 2006.

[7] J. Machann, C. Thamer, B. Schnoedt, M. Haap, H. Haring, C. Claussen, M. Stumvoll, A. Fritsche and F. Schick, "Standardized assessment of whole body adipose tissue topography by MRI.," *J Magn Reson Imaging,* vol. 21(4), pp. 455-462, April 2005.

[8] S. R. Mehta, E. L. Thomas, J. D. Bell, D. G. Johnston and S. D. Taylor-Robinson, "Non-invasive means of measuring hepatic fat content.," *World J Gastroenterol,* vol. 14(22), pp. 3476-3483, 14 June 2008.

[9] S. Reeder, P. Robson, H. Yu, A. Shimakawa, C. Hines, C. McKenzie and J. Brittain, "Quantification of hepatic steatosis with MRI: the effects of accurate fat spectral modeling.," *J Magn Reson Imaging,* vol. 29(6), pp. 1332-1339, June 2009.

[10] B. Guiu, J. Petit, R. Loffroy, S. D. Ben, S. Aho, D. Masson, P. Hillon, D. Krause and J. Cercueil, "Quantification of liver fat content: comparison of triple-echo chemical shift gradient-echo imaging and in vivo proton MR spectroscopy.," *Radiology,* vol. 250(1),

pp. 95-102, January 2009.

[11] H. Kim, S. Taksali, S. Dufour, D. Befroy, T. Goodman, K. Petersen, G. Shulman, S. Caprio and R. Constable, "Comparative MR study of hepatic fat quantification using single-voxel proton spectroscopy, two-point dixon and three-point IDEAL.," *Magn Reson Med,* vol. 59(3), pp. 521-527, March 2008.

[12] C. Liu, C. McKenzie, H. Yu, J. Brittain and S. Reeder, "Fat quantification with IDEAL gradient echo imaging: correction of bias from T(1) and noise.," *Magn Reson Med,* vol. 58(2), pp. 354-364, August 2007.

[13] K. Fumiko, M. Yuka, N. Takatomo, N. Toshio, K. Shunji, S. Seiya, H. Nobuhisa and S. Fumikazu, "Myocardial Fat at Cardiac Imaging: How Can We Differentiate Pathologic from Physiologic Fatty Infiltration?," *Radiographics,* vol. 30, pp. 1587-1602, October 2010.

[14] P. Kellman, D. Hernando and A. E. Arai, "Myocardial Fat Imaging.," *Curr Cardiovasc Imaging Rep,* vol. 3(2), pp. 83-91, April 2010.

[15] C. Y. Liu, A. Redheuil, R. Ouwerkerk, J. A. Lima and D. A. Bluemke, "Myocardial fat quantification in humans: Evaluation by two-point water-fat imaging and localized proton spectroscopy.," *Magn Reson Med,* vol. 63(4), pp. 892-901, April 2010.

[16] J. Guy, J. Mao, W. D. J. Bidgood, A. Mancuso and R. G. Quisling, "Enhancement and demyelination of the intraorbital optic nerve. Fat suppression magnetic resonance imaging.," *Ophthalmology,* vol. 99(5), pp. 713-719, May 1992.

[17] D. H. Miller, D. G. Mac Manus, P. A. Bartlett, R. Kapoor, S. P. Morrissey and I. F. Moseley, "Detection of optic nerve lesions in optic neuritis using frequency-selective fat-saturation sequences.," *Neuroradiology,* vol. 35(2), pp. 156-158, 1993.

[18] W. T. Dixon, "Simple proton spectroscopic imaging.," *Radiology,* vol. 153(1), pp. 189-194, October 1984.

[19] J. Ma, "Dixon techniques for water and fat imaging.," *J Magn Reson Imaging,* vol. 28(3), pp. 543-558, September 2008.

[20] H. N. Yeung and D. W. Kormos, "Separation of true fat and water images by correcting magnetic field inhomogeneity in situ.," *Radiology,* vol. 159(3), pp. 783-786, June 1986.

[21] G. H. Glover and E. Schneider, "Three-point Dixon technique for true water/fat decomposition with B0 inhomogeneity correction.," *Magn Reson Med,* vol. 18(2), pp. 371-383, April 1991.

[22] G. H. Glover, "Multipoint dixon technique for water and fat proton and susceptibility

imaging.," *J Magn Reson Imaging,* vol. 1(5), pp. 521-530, September-October 1991.

[23] Q. S. Xiang and L. An, "Water-fat imaging with direct phase encoding.," *J Magn Reson Imaging,* vol. 7(6), pp. 1002-1015, November-December 1997.

[24] B. D. Coombs, J. Szumowski and W. Coshow, "Two-point Dixon technique for water-fat signal decomposition with B0 inhomogeneity correction.," *Magn Reson Med,* vol. 38(6), pp. 884-889, December 1997.

[25] T. Skinner and G. H. Glover, "An extended two-point Dixon algorithm for calculating separate water, fat, and B0 images.," *Magn Reson Med,* vol. 37(4), pp. 628-630, April 1997.

[26] J. Berglund, H. Ahlström, L. Johansson and J. Kullberg, "Two-point dixon method with flexible echo times.," *Magn Reson Med,* vol. 65(4), pp. 994-1004, April 2011.

[27] H. Yu, A. Shimakawa, C. A. McKenzie, E. Brodsky, J. H. Brittain and S. B. Reeder, "Multiecho water-fat separation and simultaneous R2* estimation with multifrequency fat spectrum modeling.," *Magn Reson Med,* vol. 60(5), pp. 1122-1134, November 2008.

[28] Q. S. Xiang, "Two-point water-fat imaging with partially-opposed-phase (POP) acquisition: an asymmetric Dixon method.," *Magn Reson Med,* vol. 56(3), pp. 572-584, September 2006.

[29] S. Reeder, A. Pineda, Z. Wen, A. Shimakawa, H. Yu, J. Brittain, G. Gold, C. Beaulieu and N. Pelc, "Iterative decomposition of water and fat with echo asymmetry and least-squares estimation (IDEAL): application with fast spin-echo imaging.," *Magn Reson Med,* vol. 54(3), pp. 636-644, September 2005.

[30] A. Pineda, S. Reeder, Z. Wen and N. Pelc, "Cramér-Rao bounds for three-point decomposition of water and fat.," *Magn Reson Med,* vol. 54(3), pp. 625-635, September 2005.

[31] D. Hernando, P. Kellman, J. P. Haldar and Z. P. Liang, "Robust water/fat separation in the presence of large field inhomogeneities using a graph cut algorithm.," *Magn Reson Med,* vol. 63(1), pp. 79-90, January 2010.

[32] H. Yu, S. B. Reeder, A. Shimakawa, J. H. Brittain and N. J. Pelc, "Field map estimation with a region growing scheme for iterative 3-point water-fat decomposition.," *Magn Reson Med,* vol. 54(4), pp. 1032-1039, October 2005.

[33] J. Ma, "A single-point Dixon technique for fat-suppressed fast 3D gradient-echo imaging with a flexible echo time.," *J Magn Reson Imaging,* vol. 27(4), pp. 881-890, April 2008.

[34] E. M. Akkerman and M. Maas, "A region-growing algorithm to simultaneously remove dephasing influences and separate fat and water in two-point Dixon imaging.," in *Society*

for Magnetic Resonance in Medicine and the European Society for Magnetic Resonance in Medicine and Biology Meeting, Berkeley, California, 1995.

[35] G. Z. Yang, D. N. Firmin, R. H. Mohhiadin, J. P. Konrad and D. B. Longmore, "B0 inhomogeneity correction for two point Dixon chemical shift imaging," in *Proc., SMRM, 11th annual Meeting*, Berlin, Germany, 1992.

[36] D. Ragan and J. Bankson, "Two-point Dixon technique provides robust fat suppression for multi-mouse imaging.," *J Magn Reson Imaging*, vol. 31(2), pp. 510-514, February 2010.

[37] H. Yu, S. Reeder, C. McKenzie, A. Brau, A. Shimakawa, J. Brittain and N. Pelc, "Single acquisition water-fat separation: feasibility study for dynamic imaging.," *Magn Reson Med*, vol. 55(2), pp. 413-422, February 2006.

[38] S. Reeder, Z. Wen, H. Yu, A. Pineda, G. Gold, M. Markl and N. Pelc, "Multicoil Dixon chemical species separation with an iterative least-squares estimation method.," *Magn Reson Med*, vol. 51(1), pp. 35-45, January 2004.

[39] L. An and Q. Xiang, "Chemical shift imaging with spectrum modeling.," *Magn Reson Med*, vol. 46(1), pp. 126-130, July 2001.

[40] D. Hernando, J. Haldar, B. Sutton, J. Ma, P. Kellman and Z. Liang, "Joint estimation of water/fat images and field inhomogeneity map.," *Magn Reson Med*, vol. 59(3), pp. 571-580, March 2008.

[41] V. Chebrolu, C. Hines, H. Yu, A. Pineda, A. Shimakawa, C. McKenzie, A. Samsonov, J. Brittain and S. Reeder, "Independent estimation of T*2 for water and fat for improved accuracy of fat quantification.," *Magn Reson Med*, vol. 63(4), pp. 849-857, April 2010.

[42] M. Bydder, T. Yokoo, G. Hamilton, M. Middleton, A. Chavez, J. Schwimmer, J. Lavine and C. Sirlin, "Relaxation effects in the quantification of fat using gradient echo imaging.," *Magn Reson Imaging*, vol. 26(3), pp. 347-359, April 2008.

[43] C. Hines, H. Yu, A. Shimakawa, C. McKenzie, J. Brittain and S. Reeder, "T1 independent, T2* corrected MRI with accurate spectral modeling for quantification of fat: validation in a fat-water-SPIO phantom.," *J Magn Reson Imaging*, vol. 30(5), pp. 1215-1222, November 2009.

[44] J. Hennig, A. Nauerth and H. Friedburg, "RARE imaging: a fast imaging method for clinical MR.," *Magn Reson Med*, vol. 3(6), pp. 823-833, December 1986.

[45] R. Buxton, G. Wismer, T. Brady and B. Rosen, "Quantitative proton chemical-shift imaging.," *Magn Reson Med*, vol. 3(6), pp. 881-900, December 1986.

VYBRANÉ VLASTNÍ PUBLIKACE

KOŘÍNEK, R.; VONDRÁK, J.; BARTUŠEK, K.; SEDLAŘÍKOVÁ, M. Experimental investigations of relaxation times of gel electrolytes during polymerization by MR methods. *Journal of Solid State Electrochemistry,* 2013, roč. 17, č. 8, s. 2109-2114. ISSN: 1432- 8488.

KOŘÍNEK, R.; BARTUSEK, K. Precise Measurement of T2 Using the Turbo FLASH Method. In *Measurement 2013. Proceedings of the 9th International Conference on Measurement*. Bratislava : Institute of Measurement Science SAS, 2013, S. 191-194. ISBN 978-80-969672-5-4. [Measurement 2013. International Conference on Measurement /9./, Smolenice, 27.05.2013-30.05.2013, SK].

KOŘÍNEK, R.; BARTUŠEK, K.; OSTANINA, K.; MUSIL, M. NMR Measurement of the Relaxations and Conductivity of Gel Electrolytes. In *Proceedings of PIERS 2012 in Kuala Lumpur, March 27-30, 2012.* 2012. s. 1060-1063. ISBN: 978-1-934142-20- 2.

KOŘÍNEK, R.; BARTUSEK, K.; STARČUK, Z. Water-fat separation in rat by MRI at high field. In *Measurement 2015. Proceedings of the 10th International Conference on Measurement*. (přijato)

KOŘÍNEK, R.; DRAŽANOVÁ, E. ; BARTUŠEK, K. ; MICALE, V. ; Starčuk jr., Zenon. The brain changes of anisotropy in MAM model of schizophrenia in rat. In *Magma. Book of Abstract ESMRMB*. Vol. S1.. Berlin : Springer-Verlag, 2013, S. 294. ISSN 1352-8661. [ESMRMB 2013. Congress, Tolouse, 03.10.2013-05.10.2013, FR].